Computational evaluation of strain-rate-dependent deformation behavior of rubber and carbon-black-filled rubber under monotonic and cyclic straining

Tomita, Yoshihiro

Azuma, Keisuke

Naito, Masato

(Citation)
International Journal of Mechanical Sciences,50(5):856-868

(Issue Date)
2008-05

(Resource Type)
journal article

(Version)
Accepted Manuscript

(URL)
https://hdl.handle.net/20.500.14094/90000845

AEPA2006 Special Issue

Computational Evaluation of Strain-Rate-Dependent Deformation Behavior of Rubber and Carbon-Black-Filled Rubber under Monotonic and Cyclic Straining

Y. Tomita[1,a], K. Azuma[1,b] , M. Naito[1,2,c]

[1] Division of Mechanical Engineering, Graduate School of Engineering, Kobe University, Rokkodai 1 Nada, Kobe, 657-8501, Japan

[2]SRI & D Ltd. Tutui 2-1-1, Chuo, Kobe, 651-0071, Japan

[a]tomita@mech.kobe-u.ac.jp, [b]azuma@solid.mech.kobe-u.ac.jp,

[c]m-naito.az@srigroup.co.jp

Corresponding Address:

Professor Yoshihiro Tomita

Division of Mechanical Engineering

Graduate School of Engineering, Kobe University

Rokkodai-1 Nada Kobe 657-8501, Japan

Tel:+81-78-803-6125, Fax:+81-78-803-6155,

Email:tomita@mech.kobe-u.ac.jp

URL:http://solid.mech.kobe-u.ac.jp

Computational Evaluation of Strain-Rate-Dependent Deformation Behavior of Rubber and Carbon-Black-Filled Rubber under Monotonic and Cyclic Straining

Y. Tomita[1,a], K. Azuma[1,b] , M. Naito[1,2,c]

[1] Division of Mechanical Engineering, Graduate School of Engineering, Kobe University, Rokkodai 1 Nada, Kobe, 657-8501, Japan

[2]SRI & D Ltd. Tutui 2-1-1, Chuo, Kobe, 651-0071, Japan

[a]tomita@mech.kobe-u.ac.jp, [b]azuma@solid.mech.kobe-u.ac.jp, [c]m-naito.az@srigroup.co.jp

Key words: Strain-rate-dependent behavior, Carbon-Black-filled rubber, Cyclic deformation behavior, Hysteresis loss, Homogenization method, Molecular chain network theory

Abstract. The molecular chain network model for elastic deformation behavior and the reptation theory for viscoelastic deformation behavior are used to derive a constitutive equation for rubber. The new eight-chain-like model contains eight standard models consisting of Langevin springs and dashpot to account for the interaction of chains with their surroundings. Monotonic and cyclic deformation behavior of rubber with relaxation under different strain rates have been examined. The results reveal the roles of the individual springs and dashpot, and the strain rate dependence of materials in the monotonic and cyclic deformation behaviors, particularly softening and hysteresis loss, that is, the Mullins effect, occurring in stress-stretch curves under cyclic deformation processes. The validity of the results is checked through comparison with experimental results. The deformation behaviors of a plane strain rubber unit cell containing Carbon-Black (CB) under monotonic and cyclic straining are investigated by computational simulation using the proposed constitutive equation and homogenization method. The results reveal the

substantial enhancement of the resistance of CB-filled rubber to macroscopic deformation, which is caused by the marked orientation hardening due to the highly localized deformation of rubber. The role of strain rate sensitivity on such characteristic deformation behaviors as increases in the resistance to deformation, hysteresis loss, and the effects of the distribution morphology and the volume fraction of CB on the deformation behavior is clarified. The increases in the volume fraction and in the aggregation of the distribution of CB substantially raise the resistance to deformation and hysteresis loss.

1. Introduction

It is well known that rubber exhibits a complex deformation behavior under monotonic and cyclic straining. Hysteresis loss, that is, the Mullins effect [1] during cyclic loading processes, depends on the strain rate applied, which is strongly related to the ultimate properties of carbon-black (CB)-filled rubber [2]. Blending of CB induces a marked change in such mechanical properties as the resistance to deformation and hysteresis loss. The manifestations of hysteresis and the viscoelastic response of unfilled rubber were explained by the change in the entanglement situation of the molecular structures [3], slipping of the molecular chain [4] and the interaction of springs with the surroundings [5-7]. For the CB-filled rubber, phenomenological constitutive equations [4, 6, 8, 9] have been proposed, however, the detailes of the mechanism of the manifestation of the characteristic response caused by the microscopic deformation behavior depending on the volume fraction and distribution morphology of CB have not yet been clarified. Therefore, it is indispensable to establish a suitable constitutive equation that can reproduce the strain-rate-dependent nature of the rubber and a computational model for evaluating the effect of the CB-filling on the deformation behavior of CB-filled rubber.

Thus far, we have developed a nonaffine model that accounts for the change in the entanglement situation of the molecular network structure [10, 11] and constructed a computational model of CB-filled rubber using the proposed constitutive equation and homogenization method [12]. The strain-rate

-independent mechanical characteristics of unfilled and CB-filled rubber have been investigated [3], and the mechanism of the enhancement of the mechanical characteristics of the rubber upon filling CB have been clarified. Here, in order to reproduce the strain rate sensitivity of the response of CB-filled rubber, we develop a viscoelastic constitutive equation based on the reptation theory [5, 7] for the viscoelastic nature of the rubber and the molecular chain network theory for the nonlinear elastic response. The validity of the proposed constitutive equation will be examined against the experimental data. A unit cell model is constructed to evaluate the effect of the volume fraction and distribution morphology of CB on the deformation behavior of CB-filled rubber under different strain rate conditions. The elaborated 3D model will enable us to clarify the effect of the distribution morphology on the deformation behavior of CB-filled rubber.

2. Constitutive Equation

To duplicate the experimentally observed characteristic features of the rubber, the microstructure of rubber is assumed to consist of long molecular chains randomly distributed in space. A single chain, which consists of several segments containing monomers, is defined by two linkages, which are assumed to be chemically or physically entangled points of molecular chains. The physical links are, in general, not permanent and may change depending on deformation. On the other hand, chemical links are permanent and preserve the entanglement situation. The decrease in the number of entangled points upon deformation causes an increase in the average number of segments N in a single chain, enhanced extensibility, and a reduction in the stiffness of the material, i.e., softening, which all play very important roles in the manifestation of the hysteresis of the cyclic deformation behavior of strain-rate-independent rubber [3]. To account for the change in the number of entangled points, a nonaffine molecular chain network theory was developed [11], in which the number of entangled points is expressed as a suitable function of temperature and an appropriately defined measure of deformation. However, in this investigation, we focus our attention on the evaluation of the effect of the viscoelastic nature of the rubber on the characteristic

deformation behavior of CB-filled rubber and we restrict our attention to the affine model.

The principal deviatoric stress s_i and principal stretch λ_i relations for the eight-chain model become [13]

$$s_i = \frac{1}{3} C^R \sqrt{N} \frac{\lambda_i^2 - \lambda_c^2}{\lambda_c} L^{-1}\left(\frac{\lambda_c}{\sqrt{N}}\right), \quad L(x) = \coth x - \frac{1}{x}, \quad \lambda_c^2 = \frac{1}{3}(\lambda_1^2 + \lambda_2^2 + \lambda_3^2), \tag{1}$$

where $C^R = nk_BT$ is a constant, n is the number of chains per unit volume, k_B is Boltzmann's constant, and L is the Langevin function.

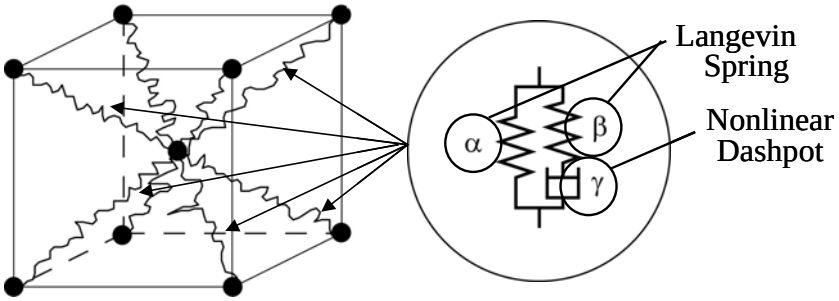

Fig. 1 Eight-chain model containing standard elements. α and β are Langevin springs and γ is dashpot.

The long molecular chains are in contact with other chains at many points, which is the potential source of the viscoelastic response. Therefore, a chain easily moves along the chain direction; however, its movement with respect to its normal direction is restricted. A tube can represent this type of restriction; upon the application of deformation, the molecular chain relaxes with respect to the chain and normal directions in a short time, and subsequently, it moves along the chain direction with long-term relaxation. This is the reptation theory that can easily account for the interaction of chains and their surroundings [5, 7]. The viscoelastic response of rubber under the application of stress σ_γ can be represented by

$$d^\gamma = \dot{\gamma}^\gamma \frac{1}{\sqrt{2}\tau^*} \sigma'_\gamma, \quad \tau^* = \left(\frac{1}{2}\sigma'_\gamma \cdot \sigma'_\gamma\right)^{\frac{1}{2}} \tag{2}$$

where d^{γ} is the viscoelastic strain rate, σ'_{γ} is the deviatoric part of σ_{γ}, and the corresponding shear strain rate $\dot{\gamma}^{\gamma}$ is a function of stretch λ_{γ} and stress τ^{*} [7].

$$\dot{\gamma}^{\gamma} = C_1\left(\lambda_{\gamma} - 1\right)^{C_2}\tau^{*m}, \quad \lambda_{\gamma} = \int_0^t \dot{\lambda}_{\gamma} dt = \int_0^t \lambda_{\gamma} d^{\gamma} dt \tag{3}$$

The material parameters C_1 and C_2 are functions of strain rate, because of the characteristic nature of chain relaxation [7].

The most typical characteristic of the present eight-chain model is that it contains eight standard models, as depicted in Fig. 1. This is because the viscoelastic response of rubber is caused by the interaction of chains with their surroundings; therefore, the component chains of the eight-chain model should exhibit a viscoelastic response. The two springs α and β represent single Langevin chains, and dashpot γ represents the viscoelastic nature of rubber, which is modeled using the reptation theory [5, 7]. With C_{α}^{R} and C_{β}^{R}, and N_{α} and N_{β} for springs α and β respectively, as in the case of the eight-chain model, we derived the relationships between stress σ_c and stretch λ_c applied to the standard model:

$$\sigma_c = C_{\alpha}^{R}\sqrt{N_{\alpha}}\,\lambda_c L^{-1}\left(\frac{\lambda_c}{\sqrt{N_{\alpha}}}\right) + C_{\beta}^{R}\sqrt{N_{\beta}}\,\frac{\lambda_c}{\lambda_{\gamma}} L^{-1}\left(\frac{\lambda_{\beta}}{\sqrt{N_{\beta}}}\right), \tag{4}$$

where $C_{\alpha}^{R} = n_{\alpha}k_B T$, $C_{\beta}^{R} = n_{\beta}k_B T$ and $n = n_{\alpha} + n_{\beta}$; n is the number of chains in the unit volume, N_{α} and N_{β} are the average numbers of segments for springs α and β, and $\sqrt{N_{\alpha}}$ and $\sqrt{N_{\beta}}$ are the corresponding limiting stretches. λ_{α}, λ_{β}, and λ_{γ} are the stretches of springs α and β, and dashpot γ, respectively, and $\lambda_c = \lambda_{\beta}\lambda_{\gamma}$. Considering the strain energy measured using the initial volume, the relationship between the principal stresses σ_i and stretches λ_i becomes

$$\sigma_i = \frac{1}{3}\left\{C_{\alpha}^{R}\sqrt{N_{\alpha}}L^{-1}\left(\frac{\lambda_c}{\sqrt{N_{\alpha}}}\right) + C_{\beta}^{R}\sqrt{N_{\beta}}\,\frac{1}{\lambda_{\gamma}}L^{-1}\left(\frac{\lambda_{\beta}}{\sqrt{N_{\beta}}}\right)\right\}\frac{\lambda_i^2}{\lambda_c} - p \tag{5}$$

where p is the hydrostatic pressure. The rate type expression of Eq. (5) provides the relationship between the Jaumann rate of Kirchoff stress $\hat{S}_{ij}$ and strain rate $\dot{\varepsilon}_{kl}$ as

$$\hat{S}_{ij} = \frac{1}{3}\left\{(\alpha_1+\beta_1)A_{ij}A_{kl}/A_{mm} + (\alpha_2+\beta_2)(\delta_{ik}A_{jl}+A_{ik}\delta_{jl})\right\}\dot{\varepsilon}_{kl} - \theta A_{ij} - \dot{p}\delta_{ij} \tag{6}$$

$$\alpha_1 = C_\alpha^R\sqrt{N_\alpha}\left(\frac{\varsigma}{\sqrt{N_\alpha}} - \frac{\tilde{L}}{\lambda_c}\right), \quad \alpha_2 = \frac{\tilde{L}C_\alpha^R\sqrt{N_\alpha}}{\lambda_c}$$

$$\beta_1 = \frac{C_\beta^R\sqrt{N_\beta}}{\lambda_\gamma}\left(\frac{\varsigma'}{\lambda_\gamma\sqrt{N_\beta}} - \frac{\tilde{L}'}{\lambda_c}\right), \quad \beta_2 = \frac{\tilde{L}'C_\beta^R\sqrt{N_\beta}}{\lambda_c}$$

$$\theta = \frac{C_\beta^R\sqrt{N_\beta}\dot{\lambda}_\gamma}{\lambda_\lambda^2\sqrt{3A_{mm}}}\left(\tilde{L}' + \frac{\lambda_\beta\varsigma'}{\sqrt{N_\beta}}\right)$$

$$\tilde{L} = L^{-1}\left(\frac{\lambda_c}{\sqrt{N_\alpha}}\right), \quad \tilde{L}' = L^{-1}\left(\frac{\lambda_\beta}{\sqrt{N_\beta}}\right)$$

$$\varsigma = \frac{\tilde{L}^2}{1-\tilde{L}^2\csc h^2\tilde{L}}, \quad \varsigma' = \frac{\tilde{L}'^2}{1-\tilde{L}'^2\csc h^2\tilde{L}'}$$

where A_{ij} is the left Cauchy-Green deformation tensor. In this investigation, the penalty method is employed to enforce the satisfaction of the volume constant deformation.

3. Deformation Behavior of Rubber

We will discuss the strain-rate-dependent nature of rubber. Fig. 2 indicates the deformation behavior of rubber under cyclic straining with constant end end velocities in the range of $100-1000mm/\min$. The experiments were performed by using thin string-like specimens with gauge length of $28.3mm$. The maximum strain rate is approximately $0.6/s$ for the end velocity $1000mm/\min$. The strain rate in the specimens decreases with the extension of the specimens under constant end velocity, which was considered in the identification of the materials parameters.

We note that material parameters C_α^R, C_β^R and N_α, N_β are deeply related to the initial elasticity moduli and limiting stretches, respectively, meanwhile, C_1, C_2 and m substantially affect strain rate dependency of the stress-stretch relation and hystelesis loss. Therefore, to avoid the effect of strain rate sensitivity of the materials C_α^R, C_β^R and N_α, N_β are determined to reproduce the stress-stretch relations for $\dot{u} = 1mm/\min$ such that the computationally predicted stress-stretch relation coincides with that due to

experiments at different stretch revels in least mean square sense. On the other hand, C_1, C_2 and m are determined by using the experimental results of stress-stretch relations and hystelesis loss with different end velocities $\dot{u} = 1, 100 mm/\min$. The detail of the determination process was the same that proposed in [14]. Thus determined materials parameters are $N_\alpha = 9.7$ and $C_\alpha^R = 0.19 MPa$ for spring α, $N_\beta = 9.5$ and $C_\beta^R = 0.21 MPa$ for spring β, and $C_1 = 7.0 \times 10^8$, $C_2 = -0.5$ and $m = 5.5$ for dashpot γ.

Fig. 2 indicates the computationally predicted deformation behavior of rubber under cyclic straining with end velocities in the range of $100 - 1000 mm/\min$. The computational simulation well reproduces the experimentally observed characteristic deformation behaviors, that is, the strain-rate-dependent hardening and the softening in the unloading process. We will use the same material parameters throughout the paper.

To clarify the strain rate dependence of the cyclic deformation behavior, the cyclic deformation behaviors under different strain rates of $10^{-3} - 10^4 / s$ are investigated in detail. Fig. 3 indicates the true stress Σ_{22}-stretch λ_2 relations under different strain rates. Increasing the strain rate causes an increase in deformation resistance. Fig. 4 shows elastic stretch λ_β and viscoelastic stretch λ_γ for the strain rates of $10^{-3} / s$, $10^2 / s$ and $10^4 / s$. For the strain rate $10^{-3} / s$, since the dashpot deforms with low resistance to deformation, the deformation of the spring is restricted, which results in the suppression of orientation hardening of the spring. As a result, the stress induced in the spring is low, which causes the lower resistance to deformation. On the other hand, at a high strain rate, $10^4 / s$, the dashpot resistance increases,

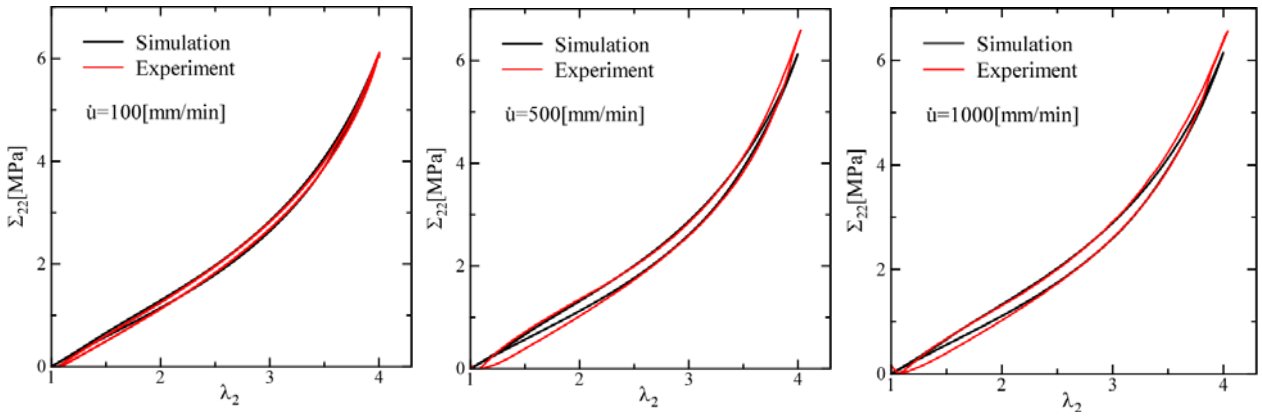

Fig. 2 True stress Σ_{22}-stretch λ_2 relationships under different end velocities.

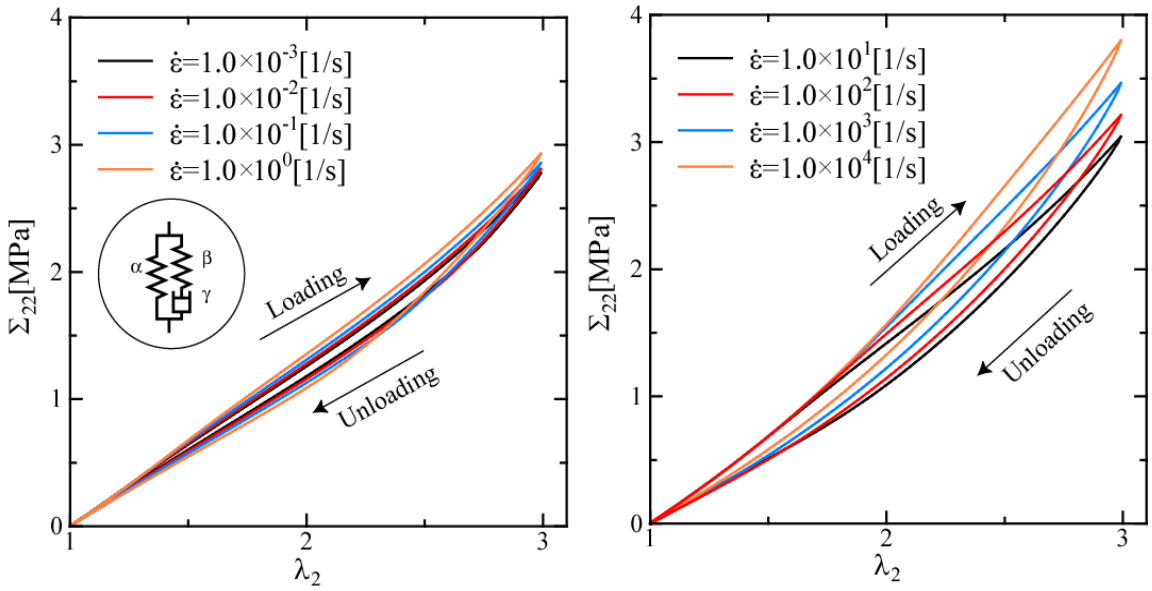

Fig. 3 Cyclic deformation behavior of rubber under different strain rates.

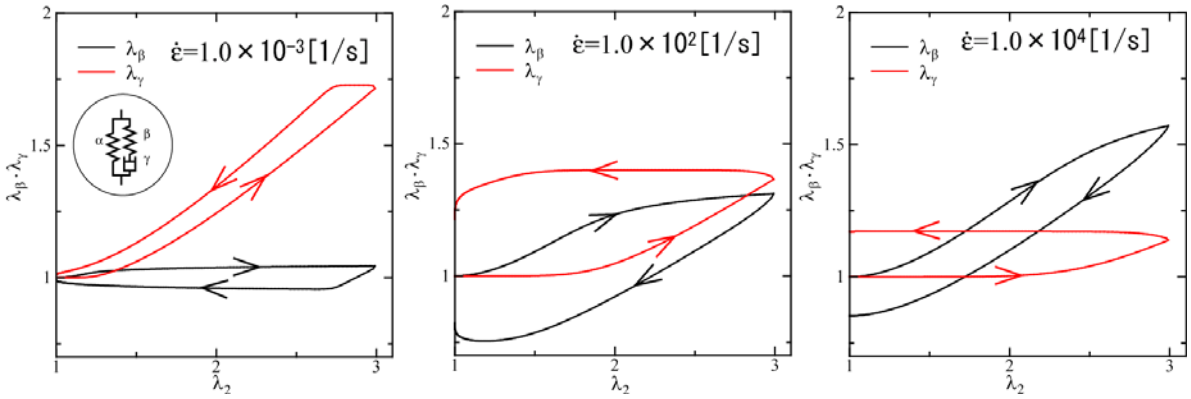

Fig. 4 Stretches of spring β and dashpot γ-stretch λ_2 relationships for different strain rates.

which promotes the deformation of the spring, with the result that the springs govern the deformation. Therefore, orientation hardening is induced and the resistance to deformation increases. With regard to the hysteresis loss defined by the area framed by loading and unloading processes, over a rather low-strain-rate region, the dashpot can deform with low stress, therefore, the deformation of the system strongly depends on spring α, which results in small hysteresis loss. With increasing strain rate, the delay of the dashpot response becomes predominant, resulting in the increase of residual stress in the unloaded state, which causes stress softening and hysteresis loss. In the high-rate-of-strain region, the resistance of the dashpot increases, therefore, the response of the system becomes elastic, which causes the reduction of hysteresis

loss. As a result, hysteresis loss is a maxima at a specific strain rate, as indicated in Fig. 5, which represents the strain- and stretch-dependent hysteresis loss.

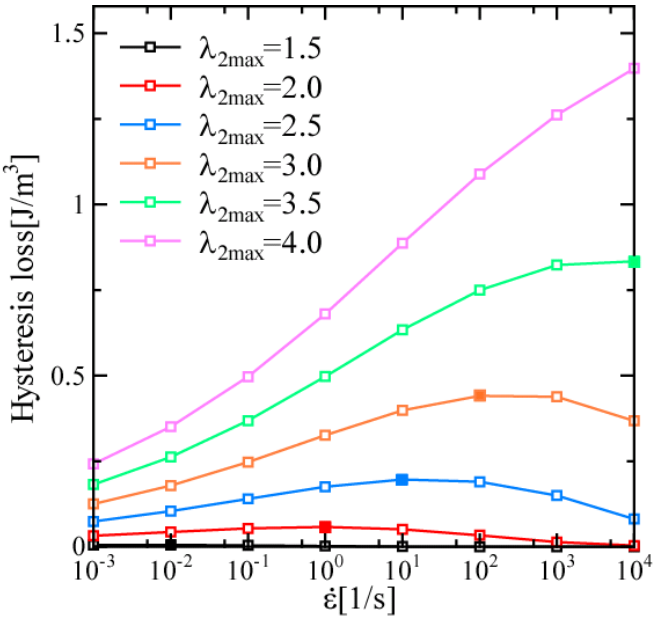

Fig. 5 Strain rate and stretch-dependent hysteresis loss

The hysteresis loss clearly depends on the stretch, as depicted in Fig. 5. With increasing stretch, the maxima of hysteresis loss appear in a the higher strain rate range. This is attributable to the increase in stress owing to orientation hardening of the spring that promotes the further deformation of the dashpot. In the localized deformation in the rubber phase of CB-filled rubber, such strain rate and stretch dependences of hysteresis loss play the central role in the characteristic deformation behavior, which will be discussed below.

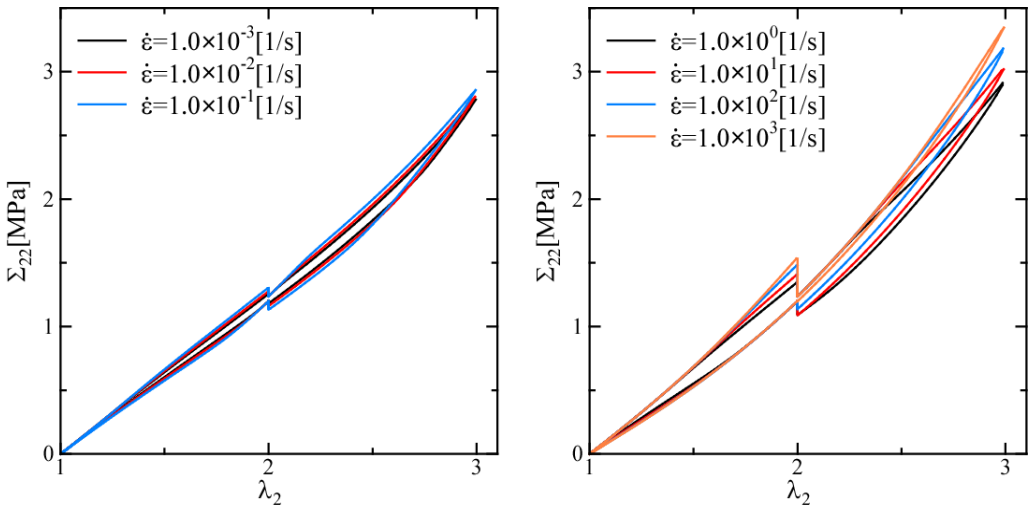

Fig. 6 Stress relaxation under different strain rates.

Fig. 6 indicates the stress relaxation behavior for different strain rates at $\lambda_2 = 2$ for the duration of 300 seconds. Due to the continuous deformation of the dashpot, the stress relaxation occurs in accordance with strain rate and loading and unloading. At a low strain rate, marked stress softening and hardening occur in the loading and unloading processes, respectively. On the other hand, at a high strain rate, stress relaxation is marked during the loading process. However, in the unloading process, it almost disappears, which can be explained using Fig. 7 which indicates the roles of the nonlinear spring and dashpot under low and high strain rates with the 300 second duration of holding stretch constant at 2. With this time duration, in the case of a low strain rate, viscoelastic stretch λ_γ increases and decreases in the loading and unloading processes, respectively. Correspondingly, elastic stretch λ_β decreases and increases, which results in softening and hardening, in the loading and unloading processes, respectively. On the other hand, for the case of high strain rate, because of the high resistance to deformation of the dashpot, elastic deformation is predominant, therefore, the dashpot deforms during this 300-second duration, which results in greater softening as compared with low-strain-rate cases in loading processes. Viscoelastic stretch λ_γ almost maintains its value during subsequent loading and unloading to the stretch where time duration was applied during the loading process. The stress applied to the dashpot is almost zero; therefore, the further change of

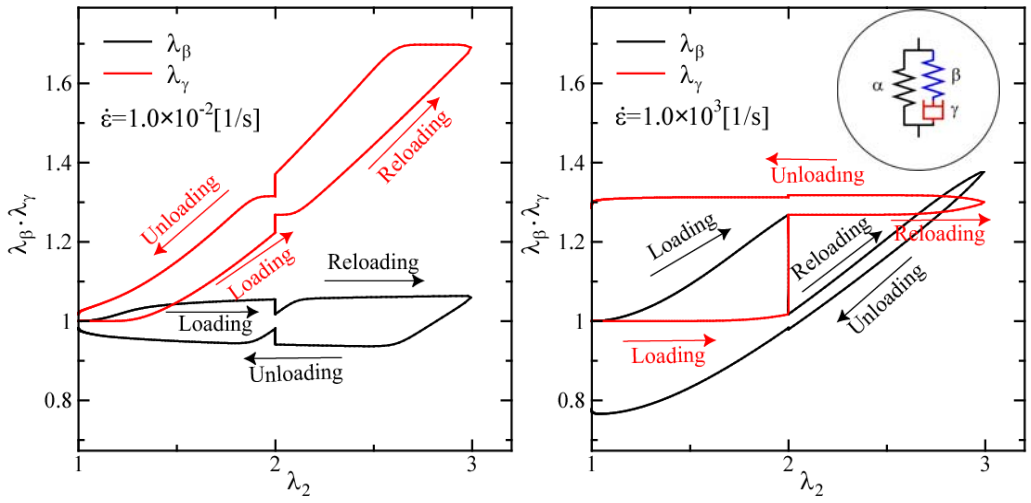

Fig. 7 Deformation of spring β and dashpot γ.

viscoelastic stretch in the time duration is unappreciable. Correspondingly, the stress increase due to the application of this time duration of constant stretch during the unloading process is low. Fig. 8 indicates the stress relaxation during loading and unloading processes with time. As mentioned previously, stress relaxation increases with the strain rate for loading processes, whereas it decreases with increasing strain rate for unloading processes.

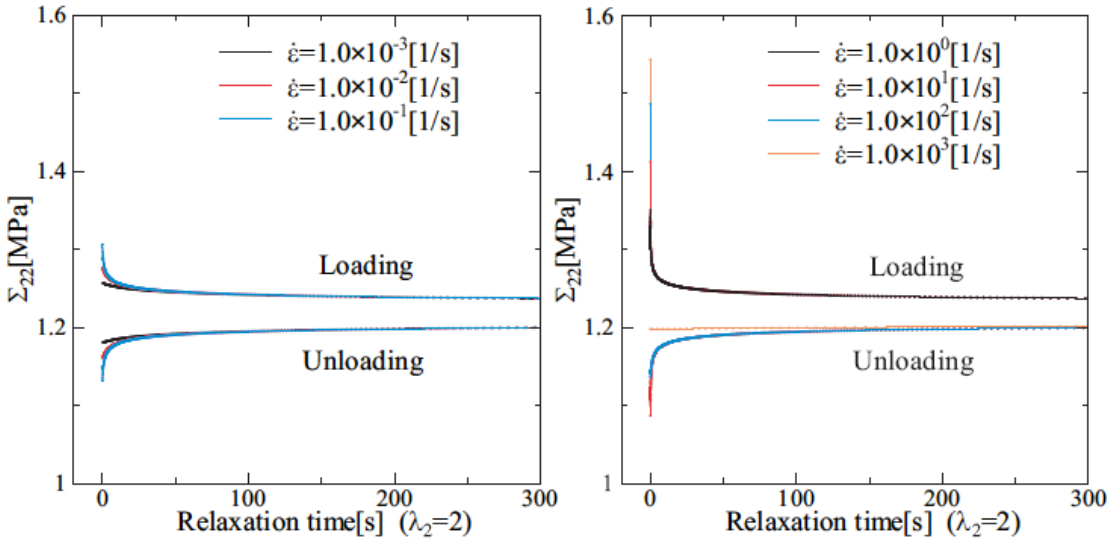

Fig. 8 Stress relaxations with time.

4. Deformation Behavior of CB-Filled Rubber

Although the distribution of CB ranges from somewhat aggregated to random, we focus our attention on the characterization of the essential effect of filling CB on the mechanical characteristics of CB-filled rubber. Fig. 9 shows the plane strain computational model in which heterogeneous CB is assumed to be distributed periodically. Here, the rubber obeys the explained constitutive equation and CB obeys the linear elastic constitutive equation. For CB, elasticity modulus and Poisson's ratio are $E_c = 100MPa$, $\nu_c = 0.3$, respectively. We employed the homogenization method [3, 12] to correlate the micro- and macroscopic deformation behaviors. The unit cell is sufficiently small as compared with the dimension of the entire body and so called Y-periodicity is assumed [15]. The present investigation is restricted the deformation

behavior of the unit cell in the entire body which uniformly deforms with boundary conditions shown in Fig.9. The top and bottom surfaces are shear-free with a constant displacement constraint, whereas the right and left surfaces are assumed to be stress-free. Thus, macroscopically homogeneous deformation is concerned, single finite element for macroscale satisfying boundary conditions for entire body is used.

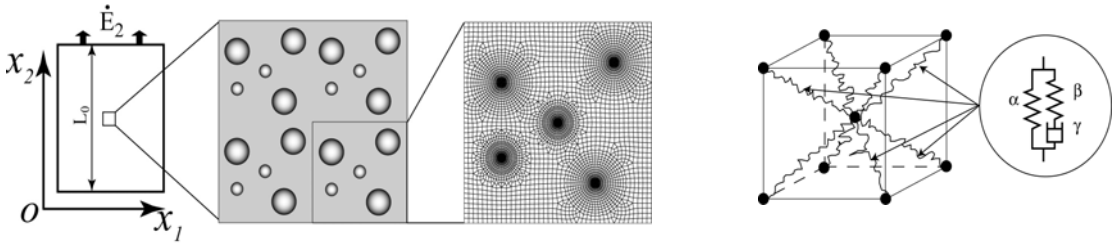

Fig. 9 Plane strain finite element model of CB-filled rubber.

Volume Fraction of CB: 20%, applied strain rate: $1.0\times10^{-3}-1.0\times10^{3}[1/s]$.

Fig. 10 indicates the stress-stretch relationships for CB-filled rubber under cyclic straining with different strain rates. For comparison, the stress-stretch relationships for unfilled rubber are also indicated. As in the case of strain rate independent rubber [3], filling with CB causes marked increases in the resistance to deformation, which is closely related to the localized deformation in the rubber phase that results in high

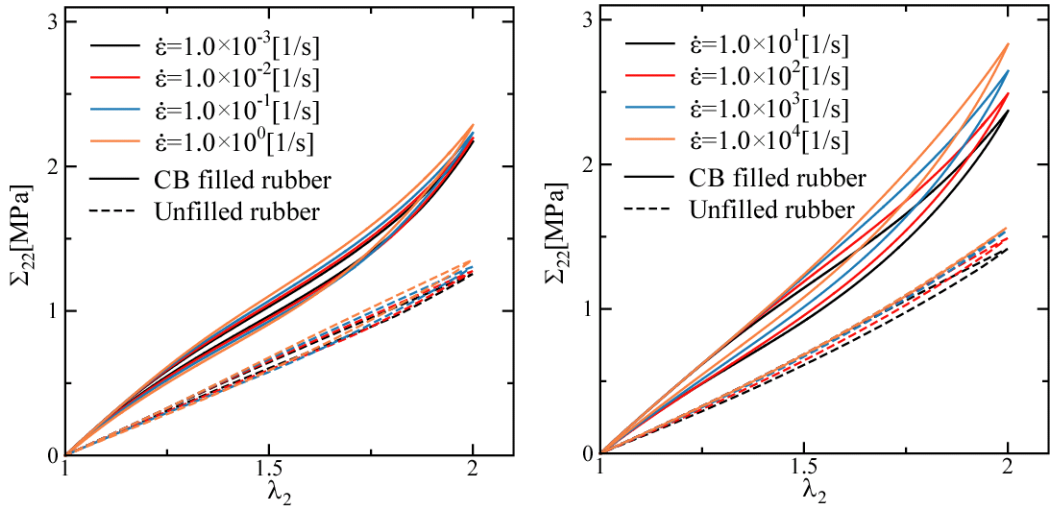

Fig. 10 Strain-rate-dependent-cyclic stress-stretch relationships of CB-filled rubber.

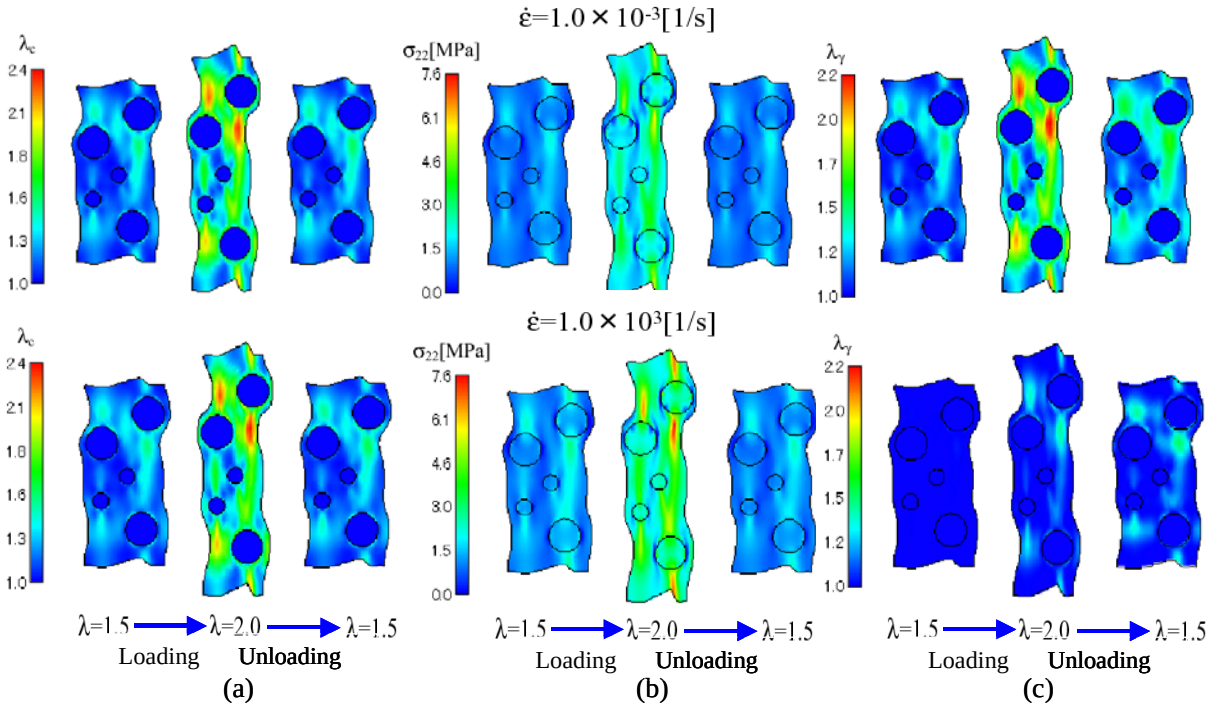

Fig. 11 Cyclic deformation behavior of CB-filled rubber. (a) Stretch λ_c, (b) tension directional stress σ_{22}, and (c) viscoelastic stretch λ_γ under different strain rates and at different deformation stages.

orientation hardening. This is the main mechanism of the enhancement of the resistance of deformation in CB-filled rubber. Additionally, increasing of strain rate raises the resistance to deformation, which can be predicted from on the strain-rate-dependent characteristics of rubber described in section 3.

Next we will show the details of the cyclic deformation behavior of CB-filled rubber under different strain rates. Fig. 11 indicates stretch λ_c, tension directional stress σ_{22} and viscoelastic stretch λ_γ distributions for different strain rates in loading and unloading stages, respectively. Fig. 11 (a) indicates that highly localized stretch regions connect the particles, which causes the marked orientation hardening that results in the marked increase in deformation resistance in CB-filled rubber. Rather low stretch regions are observed near CB. Such regions develop to bridge the highly deformed area and the remaining area by large rotation [3]. A small but recognizable difference between the same deformations in the loading and unloading stages is attributable to the Mullins effect. Fig. 11(c) indicates the effect of the strain rate dependence on the deformation behavior. At a low strain rate, high viscoelastic stretch λ_γ occurs in

localized deformation regions, which suppresses the contribution of spring β to deformation and enforces the spring-α-predominant deformation. At a high strain rate, the high resistance of the dashpot to deformation additionally promotes elastic deformation, which causes the high orientation hardening that results in the high resistance to deformation.

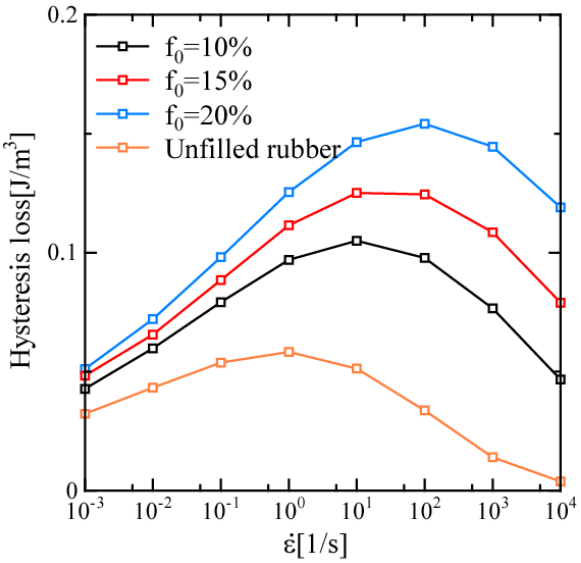

Fig. 12 Stretch-dependent hysteresis losses under different strain rates.

Fig. 12 indicates the hysteresis loss of the rubber and CB-filled rubber with respect to the strain rate. This figure clearly indicates the effect of strain rate on hysteresis loss. The peak value for CB-filled rubber is quite high compared with that of unfilled rubber. The concentration of the deformation promotes strain-rate

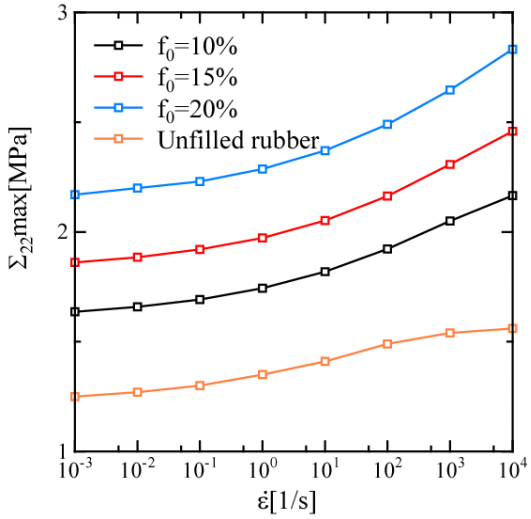

Fig. 13 Effect of CB volume fraction on stress at stretch 2.0.

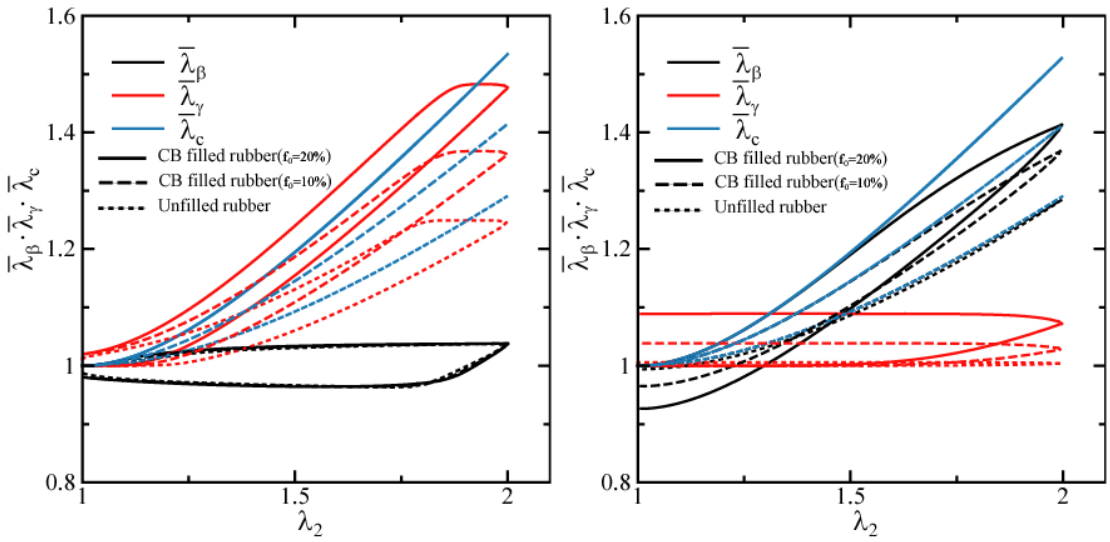

Fig. 14 Average values of stretches $\bar{\lambda}_c$, $\bar{\lambda}_\beta$ and $\bar{\lambda}_\gamma$ -stretch λ_2 relationships for different CB-volume fractions.

-dependent hysteresis loss. However, due to the highly nonuniform deformation, the location of the maximum hysteresis loss and its magnitude are different from those of unfilled rubber. The localized deformation plays the central role in the increase of the hysteresis loss of CB-filled rubber.

Fig. 13 indicates the effect of the volume fraction of CB on the stress at stretch 2.0. The resistance to deformation is intensified by increasing the volume fraction of CB; this can be explained by inspecting Fig. 14, which indicates the average values of stretch $\bar{\lambda}_c$, $\bar{\lambda}_\beta$ and $\bar{\lambda}_\gamma$ -stretch λ_2 relations. For the case of a low strain rate, $\bar{\lambda}_c$ and $\bar{\lambda}_\gamma$ increase with increasing amount of CB, therefore, $\bar{\lambda}_\gamma$ dominates stretch, which results in the suppression of orientation hardening. For a high strain rate, the contribution of $\bar{\lambda}_\gamma$ to deformation is unappreciable. As a result, elastic stretch becomes predominant and, therefore, orientation hardening proceeds. Consequently, at a low strain rate, the increase of stretch due to localization is responsible for the increase in the resistance to deformation, whereas in the high-strain-rate region, the suppression of the viscoelastic stretch due to the high resistance to deformation is additionally responsible for the increase in the resistance to deformation. The increases in hysteresis loss with increasing of CB volume fraction is attributable to the higher localization of deformation that results in the high stretch that

causes the increase of stress and promotes an additional viscoelastic stretch in the corresponding area which in turn increases the hysteresis loss as indicated in Fig. 12.

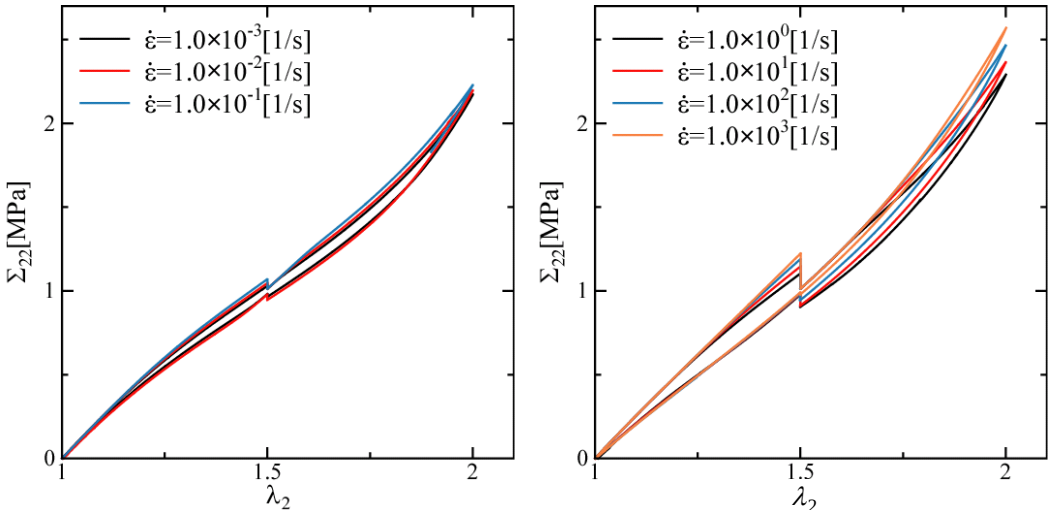

Fig.15 Stress-stretch relationships with stress relaxation under different strain rate.

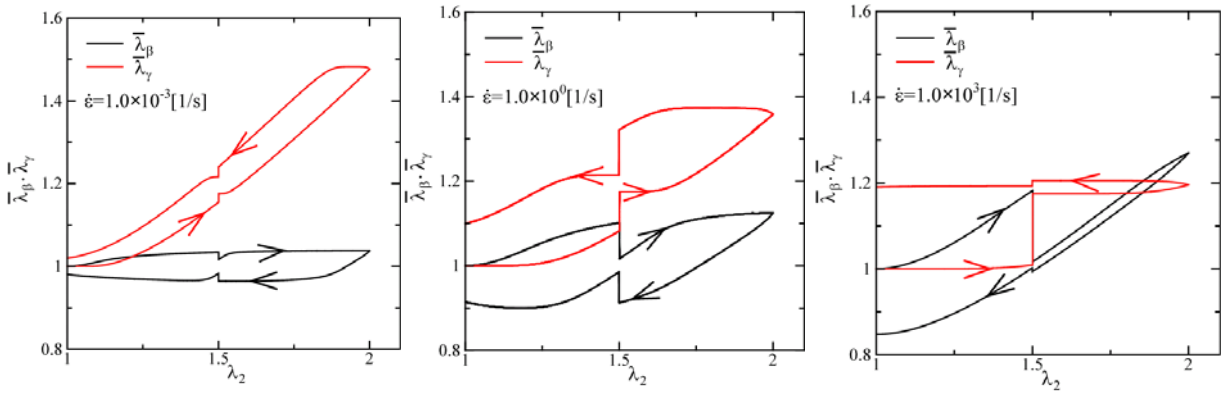

Fig.16 Average stretches, $\bar{\lambda}_\beta$, $\bar{\lambda}_\gamma$ -stretch λ_2 relationships with stress relaxation under different strain rates.

Figs. 15-17 show the stress relaxation of CB-filled rubber for different strain rates at $\lambda_2 = 1.5$ for the duration of 300 seconds. Although the locally nonuniform deformation causes a complicate response, the essential characteristic strain-rate-dependent stress relaxation behavior as discussed for CB-unfilled rubber and shown in Figs. 6, 7 and 8, can be observed. Figs. 18 and 19 indicate the tensile directional stress σ_{22} and viscoelastic stretch λ_γ in unrelaxed and relaxed states for different strain rates in loading and unloading processes. At a high strain rate, λ_γ remained low during the deformation, which causes a high

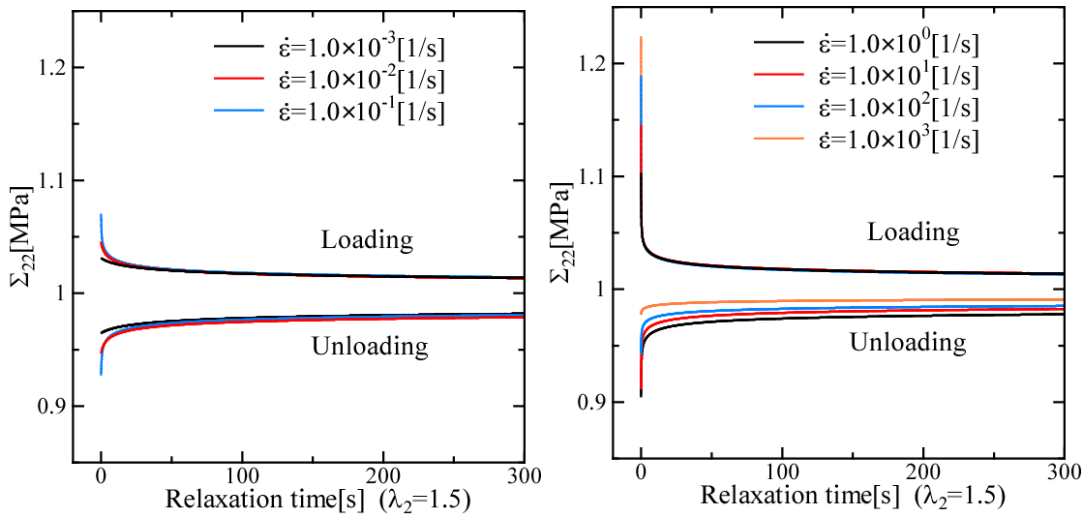

Fig.17 Stress relaxation with time under different strain rates.

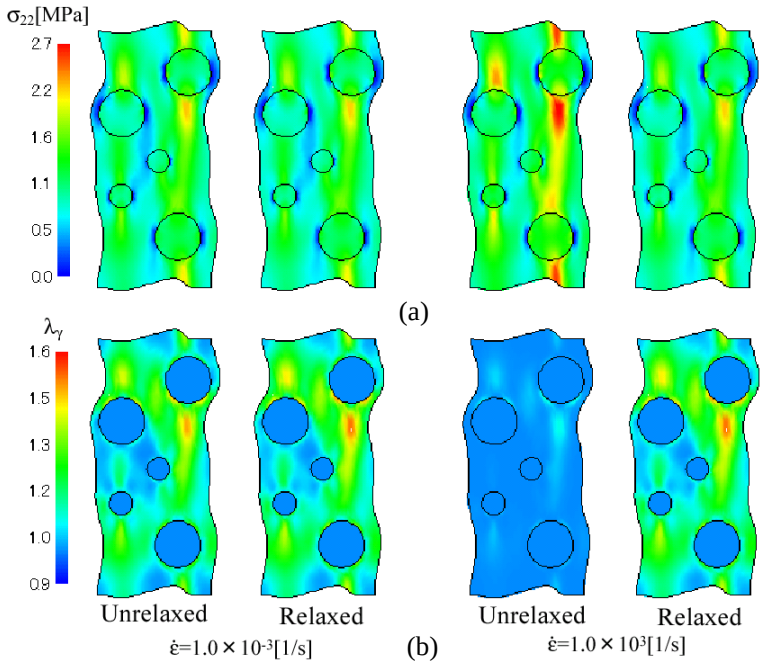

Fig.18 Stress relaxation with time under different strain rates during loading. (a) Tensile directional stress σ_{22} and (b) viscoelastic stretch λ_γ distributions with strain rates of $10^{-3}/s$ and $10^{3}/s$.

driving stress for the dashpot and results in greater relaxation of stress. This particularly marked in the high stress localization region. Incontrast, at a low strain rate, the relaxation of the dashpot proceeds during the deformation process and the relaxation in the time duration is not significant. Thus, the characteristic deformation behavior discussed for CB-unfilled rubber is intensified in the localized deformation region.

However, the total response of CB-filled rubber is homogenized one over the unit cell, therefore, it becomes moderate compared with that of CB-unfilled rubber.

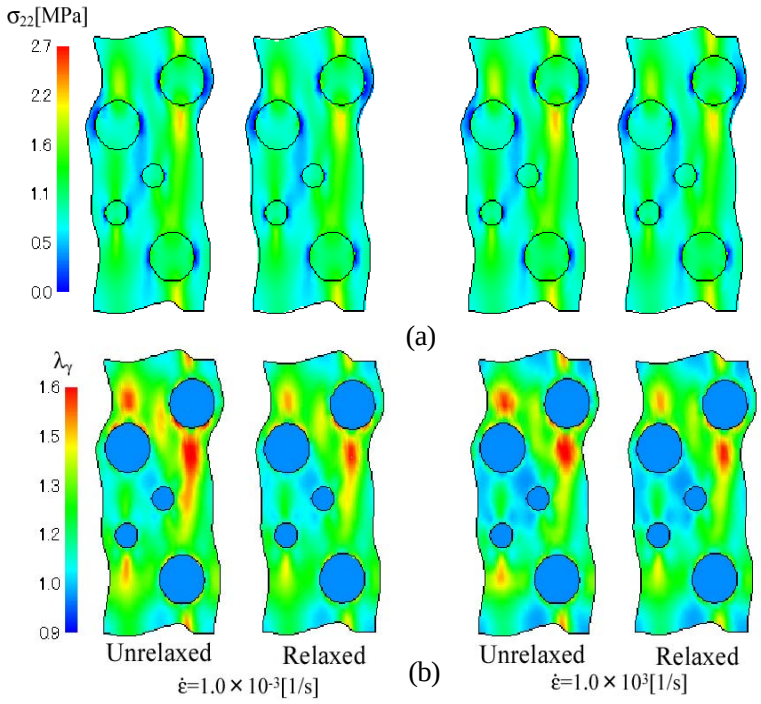

Fig.19 Stress relaxation with time under different strain rate during unloading. (a) Tensile directional stress σ_{22} and (b) viscoelastic stretch λ_γ distributions with strain rates of $10^{-3}/s$ and $10^{3}/s$.

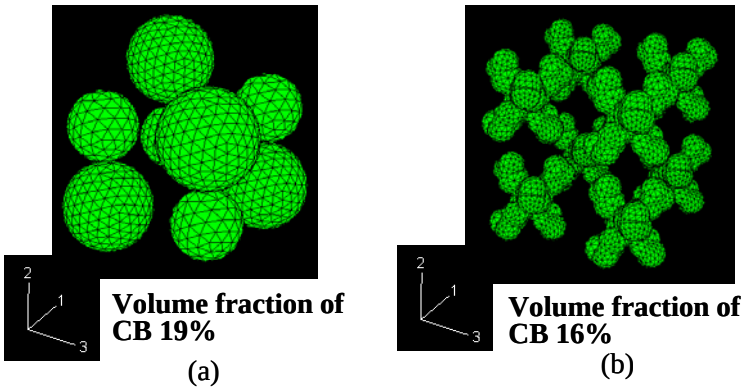

Fig. 20. 3D Computational models for different structures of CB-filled rubber.

(a) Dispersed case. (b) Aggregated case.

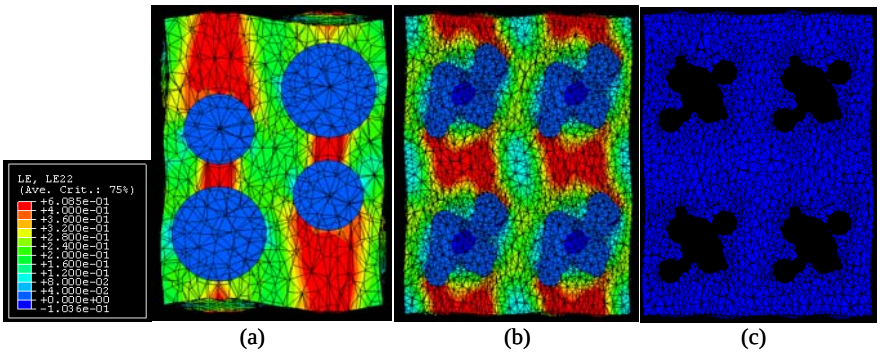

Fig. 21. Stretch distribution for (a) Dispersed case and (b) Aggregated case, and (c) CB distribution for cross-sectional area corresponding to (b).

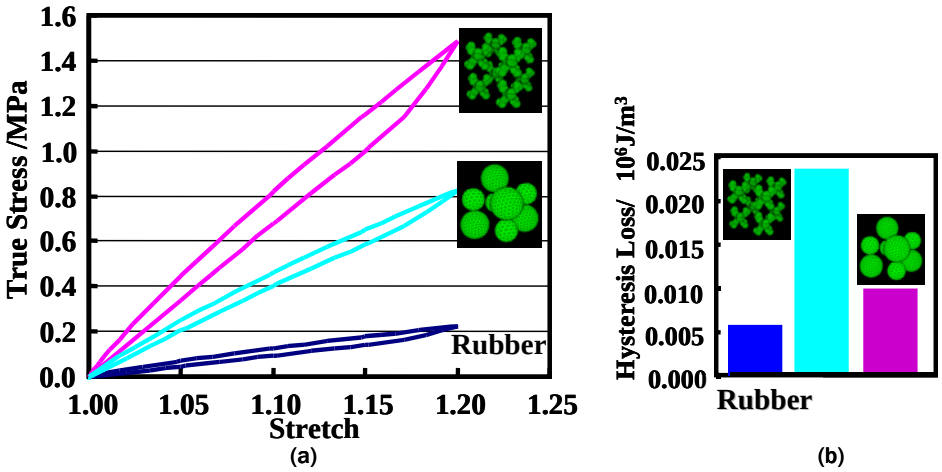

Fig. 22 Effect of CB structure on deformation behavior. (a) Stress-stretch relationships and (b) hysteresis loss for different CB distributions.

So far, we have restricted our attention to the characteristic deformation behavior of CB-filled rubber by employing a rather simple two-dimensional model. Next, we mention the deformation behavior of CB-filled rubber employing elaborate 3D models. In order to investigate the effect of the structure of CB, we present the two different 3D models depicted in Fig. 20. These correspond to dispersed and aggregated CB distributions. Figs. 21 (a), (b) and (c) indicate the stretch distributions for the dispersed and aggregated cases, and the CB distribution profile of the cross section corresponding to (b), respectively. Fig. 22 indicates the stress-stretch relationships and hysteresis losses for these cases. For comparison, the stress-stretch relationship for unfilled rubber is also indicated. There are marked increases in the resistance

to deformation during the loading processes and in the hysteresis loss of the CB-filled rubber. The local concentration of the deformation due to the existence of CB causes much stretching, as indicated in Figs. 21 (a) and (b), which results in high orientation hardening and deformation-induced softening. Therefore, as mentioned previously, the resistance to deformation and the hysteresis loss for CB-filled rubber are markedly increased compared with those for unfilled rubber. The volume fraction of CB in the aggregated case is lower than that in the dispersed case. Nevertheless, the aggregated case exhibits much higher resistance to deformation and hysteresis loss. As indicated in the aggregated case, Fig. 21 (b), very highly concentrated deformation areas are observed. It should be noted that very low deformation regions surrounding the aggregated CB are seen in Fig.21 (b). Such regions act to increase the net CB volume fraction as indicated in Fig. 21(c), and additionally intensifies the concentration of orientation hardening. The effect of aggregated distributions of fibers, fiber clustering, in metal matrix composites subjected to small strain was investigated [16,17]. It was clarified that the common mechanism in these cases is the suppression of the effective stress within the fiber/inclusion cluster, thereby effectively increasing the apparent fiber/inclusion volume fraction [17]. Due to the characteristic anisotropic hardening behavior caused by orientation of molecular chains, viscoelastic nature of the materials and very large deformation that causes the morphological change of CB distributions the CB-filled rubber deforms in very complex way. Therefore, the individual contributions on the deformation are hard to clarify, however, the effect of micromechanical distribution of stress, stretch and rotation of rubber on the macroscopic deformation behavior is seen in [3]. Thus, apart from detailed microscopic deformation, the similar contribution of aggregated distribution of particles on the resistance to deformation is seen [16,17].

The obtained results clarify the essential physical enhancement mechanisms of deformation resistance and hysteresis loss that are dependent on the volume fraction, distribution and filler size, and provide important information for the design of CB-filled rubber with high strength and functionality.

5. Conclusions

We developed a viscoelastic constitutive equation for rubber and a computational model of the monotonic and cyclic deformation behavior of CB-filled rubber by means of the homogenization method and the proposed constitutive equation. A series of simulations has revealed the typical characteristic deformation behavior of the rubber and the mechanisms of the enhancement of the characteristic mechanical behavior of CB-filled rubber.

First, for unfilled rubber, a new constitutive equation based on an eight-chain model in which eight Langevin springs are replaced by standard models consisting of Langevin springs and a dashpot was proposed. The viscoelastic nature of the rubber was modeled using reptation theory. The typical strain-rate-dependent deformation behaviors under monotonic and cyclic straining with different strain rates were reproduced and they corresponded well to the experimentally obtained results. At a low rate of deformation, because of the low viscoelastic resistance, the orientation hardening of the Langevin spring was suppressed. With increasing strain rate, which causes the increase of dashpot resistance, the deformation behavior tends to be governed by the Langevin spring, and orientation hardening is promoted. Therefore, hysteresis loss attributable to the strain rate sensitivity of the rubber has a maximum at a specific strain rate that depends on stretch. The stress relaxation behavior under different strain rates of deformation is unique, that is, because of viscoelastic resistance, stress relaxation proceeds during deformation at a low strain rate. Conversely, it is suppressed at a high strain rate, which results in marked stress relaxation with time.

In the case of CB-filled rubber, without any additional material parameters, the present model well reproduces the marked increases in the resistance of deformation and the Mullins effect, which is closely related to the orientation hardening in the rubber caused by the highly localized deformation due to filling with CB. That is, the marked enhancement of orientation hardening and the promotion of the viscoelastic nature of the rubber results in the magnification and strain rate dependence of the hysteresis loss in

stress-stretch curves under the cyclic deformation behavior. In particular, localized deformation promotes the orientation hardening that causes the increase of the stress which in turn results in further viscoelastic deformation and increase in hysteresis loss. Correspondingly, an increase in the volume fraction of CB markedly enhances this characteristic behavior. The local stress relaxation behavior of CB-filled rubber is very complicated and depends on the localization of deformation and the interaction with the surroundings. However, the homogenized response is moderate compared with that of unfilled rubber.

The elaborated 3D model of CB-filled rubber was used to clarify the effect of the distribution morphology of CB. An aggregated distribution of CB suggested the presence of nondeformed regions and the existence of an effective volume of CB, which reduces the net deforming region and markedly promotes local deformation and enhances the resistance to deformation and the hysteresis loss.

Acknowledgements. Financial support from the Ministry of Education, Culture, Sports, Science and Technology of Japan through a Grant-in-Aid for Scientific Research is highly appreciated. We are also grateful for the financial support from SRI R&D Ltd.

References

[1] Mullins L. Softening of rubber by deformation. Rubber Chem Technol 1969; 42: 339–361.

[2] Mullins L. Effect of stretching on the properties of rubber. J Rubber Res 1947; 16: 275–289.

[3] Tomita Y, Lu Wei, Naito M, Y. Furutani. Numerical Evaluation of Micro- to Macroscopic Mechanical Behavior of Carbon-Black-Filled Rubber. Int J Mech Sci 2006; 48(2): 108-116.

[4] Dannenberg EM. The effect of Surface Chemical Interface on the properties of Filler-Reinforced Rubber. Rubber Chemistry and Technology 1975; 48: 410-444.

[5] Doi M, Edwards SF. The Theory of Polymer Dynamics.1986; 16-28. Oxford University Press.

[6] Fukahori Y. The Dynamics of a Macromolecule for a Design. 2000, Gihoudoushuppan, in Japanese.

[7] Bergstrom JS, Boyce MC. Constitutive modeling of the large strain time-dependent behavior of

elastomers. J Mech Phys Solids 1998; 46: 931-954.

[8] O'Brien J, Cashel E, Wardell GE, McBrierty V. An NMR Investigation of the Interaction between Carbon Black and cis-Polybutadiene. Macromolecules 1976; 9(4): 653-660.

[9] Bergstrom JS, Boyce MC. Large strain time-dependent behavior of filled elastomers. Mech Mater 2000; 32: 627-644.

[10] Tomita Y, Tanaka S, Prediction of deformation behavior of glassy polymers based on molecular chain network model. Int J Solids & Structures 1995; 32(23):3423-3434.

[11] Tomita Y, Adachi T, Tanaka S, Modelling and application of constitutive equation for glassy polymer based on nonaffine network theory. Eur J Mech A/Solids 1997;16: 745-755.

[12] Higa Y, Tomita Y, Computational prediction of mechanical properties of nickel-based superalloy with gamma prime phase precipitates. Advance Materials and Modeling of Mechanical Behavior, **III**, 1999; 1061-1066, eds. F. Ellyin and J.W. Provan, Fleming Printing Ltd., Victoria, B.C., Canada .

[13] Arruda EM, Boyce MC, A three-dimensional constitutive model for large stretch behavior of rubber materials. J Mech Phys Solids 1993; 41: 389-412.

[14] Tomita Y, Adachi T, Park SS, Computational simulation of three-dimensional neck propagation in polymeric specimens under tension and hybrid identification of constitutive equation. Int J Mech Sci 1997; 39; 913-923.

[15] Guedes JM Kikuchi N, Preprocessing and postprocessing for materials based on the homogenization method with adaptive finite element method. Compt Meth Appl Mech Engng 1990; 83; 143-198.

[16] Conlon KT, Wilkinson DS, Effect of Particle Distribution on Deformation and Damage of Two-Phase Alloys, Materials Sci Engng 2001; A317, 108-114.

[17] Bansal Y, Pindera MJ, Finite-Volume Direct Averaging Micromechanics of Heterogeneous Materials with Elastic-Plastic Phases, Int J Plasticity 2006; 22; 775-825.